Anomalous slip in body-centred cubic metals

Daniel Caillard, Baptiste Bienvenu, Emmanuel Clouet

Anomalous slip in body-centred cubic metals

Daniel Caillard[1*], Baptiste Bienvenu[2] & Emmanuel Clouet[2*]

[1] *CEMES-CNRS, 29 rue Jeanne Marvig, BP 94347, 31055 Toulouse, France*

[2] *Université Paris-Saclay, CEA, Service de Recherches de Métallurgie Physique, Gif-sur-Yvette 91191, France*

[*] *Corresponding authors.*

Crystal strength and plastic flow are controlled by the motion and interaction of dislocations, the line defects carrying atomic shear increments. While, in most crystals, deformation develops in the crystallographic planes where the glide force acting on dislocations is maximum, plasticity in body-centred cubic (BCC) metals is more complex. Slip systems where the resolved shear stress is not the highest can dominate at low temperature, leading to anomalous slip[1,2]. Using in situ tensile tests in a transmission electron microscope we show that anomalous slip arises from the high mobility of multi-junctions[3], i.e. junctions between more than two dislocations, which glide at a velocity several orders of magnitude larger than single dislocations. These multi-junctions result from the interaction of a simple binary junction with a gliding dislocation. Although elasticity theory predicts that these binary junctions should be unstable in crystals with a weak elastic anisotropy like tungsten, both experiments and atomistic simulations reveal that such junctions can be created under dynamic conditions, in agreement with the existence of anomalous slip in almost all BCC metals, including tungsten[4,5].

Anomalous slip is a long standing and still unsolved problem in the field of the mechanical properties of body centred cubic (BCC) metals. First observed in niobium[6] and since then extensively studied in different BCC metals (Extended Data Tab. 1), it is characterized by the occurrence of long and straight slip bands in non-expected $\{110\}$ planes with low resolved shear stresses, namely in planes where dislocations are subjected to quite low driving forces, about two-times lower than for the primary slip system. This is clearly at variance with the usual behaviour, also observed beside anomalous slip, where wavy and non-crystallographic slip bands correspond to the most activated slip systems.

Anomalous slip exhibits several characteristic features giving precious indications about its possible origin. First, slip bands are very planar and without so-called "dead bands": when observed around samples with rounded section, the slip band contrast only decreases along a direction, which is intermediate between the two $1/2\,\langle 111\rangle$ shear directions contained in the anomalous slip plane, and does not vanish, as expected when the shear direction is locally parallel to the surface. Anomalous slip thus corresponds to the cooperative motion of dislocations with two different $1/2\,\langle 111\rangle$ Burgers vectors, both belonging to the anomalous $\{110\}$ slip plane. Second, anomalous slip is observed in both tension and compression, which rules out interpretations based on the role of non-glide stresses, e.g. stresses normal to the slip plane, on dislocation mobility[2,7,8]. It is also prominent for directions of tensile or compressive axes in the centre of the $\langle 001\rangle - \langle 011\rangle - \langle 111\rangle$ stereographic triangle. Third, anomalous slip takes place only at low temperature in very pure materials, where dislocations align along the direction parallel to their Burgers vector because of the high lattice friction experienced by this screw orientation. In addition, TEM observations in Nb and Mo show that straight screws are most often arranged in networks parallel to the anomalous slip bands[9,10,11,12,13]. These planar networks contain the two screw families activated in the bands, which react to form junctions with $\langle 100\rangle$ Burgers vectors.

Proposed models of anomalous slip are based either on surface effects easing glide of dislocations in the anomalous planes[5,9,14] or on the presence of the above-mentioned planar networks. As pointed by Tayor[15], surface effects fail to account for all characteristics of anomalous slip, in particular the activation of two dislocation families. In models based on planar networks, the two dislocation families composing the network are assumed to move cooperatively in the anomalous plane, at a lower applied stress than isolated dislocations thanks to the easiest nucleation of kinks on screw dislocations at the network nodes[16,17,18,19]. In situ straining experiments in a transmission electron microscope (TEM) have shown that such a cooperative motion of dislocations inside the network do exist[9,20]. However, the networks observed in TEM are so imperfect that it is difficult to imagine how they could glide as a whole over long distances. One thus still does not fully understand the exact origin of anomalous slip in BCC metals.

Our in situ TEM straining experiments performed in niobium show the usual low-temperature plastic behaviour of BCC metals. Screw dislocations belonging to four different families glide slowly and steadily in non-crystallographic slip planes (Extended Data Fig. 1), in agreement with a motion controlled by the nucleation of kink-pairs. Their average velocity is of the order of 5 nm/s. Dislocation networks are also identified (Extended Data Fig. 2). They are made of two interacting screw dislocation families with Burgers vectors $\vec{b}_1 = 1/2\,[\bar{1}1\bar{1}]$ and $\vec{b}_2 = 1/2[111]$ which form junctions with Burgers vector $\vec{b}_{JR} = [010]$. These networks glide in the plane $P_{12} = (10\bar{1})$ containing the three dislocation families, with a velocity of about 15 nm/s for the fastest nodes, only slightly higher than neighbouring isolated screw dislocations. Networks are thus not much more mobile than individual dislocations. The often-proposed mechanism, with easy kink nucleation at the nodes leading to fast glide of the network in the anomalous slip plane, is thus inoperative in real situations where dislocation networks are not perfectly planar.

Surprisingly, our experiments also reveal a completely different and new behaviour, a very fast motion of a group of four straight screw dislocations connected at a single node (Fig. 1a-c). These dislocations glide cooperatively over large distances at a velocity higher than 50 μm/s, thus several orders of magnitude higher than individual dislocations. This fast motion is generally issued from a dense region containing tangles of two or more dislocation families and leaves two sets of horizontal traces at the two foil surfaces corresponding to the two orthogonal glide planes $P_{12} = (10\bar{1})$ and $P_{34} = (101)$. Twenty similar events have been recorded in different Nb samples (see Extended Data Fig. 3 for some more examples), showing that such a motion is not unusual. The four screw dislocations connected at the node have necessarily different Burgers vectors that sum up to zero, explaining why no dislocation is left behind after the node has glided. Relaxing in atomistic simulation such a node connecting four screw dislocations with Burgers vectors $\vec{b}_1 = 1/2\,[\bar{1}1\bar{1}]$, $\vec{b}_2 = 1/2\,[111]$, $\vec{b}_3 = 1/2\,[1\bar{1}\bar{1}]$ and $\vec{b}_4 = -\vec{b}_1 - \vec{b}_2 - \vec{b}_3 = 1/2\,[\bar{1}\bar{1}1]$, one sees that the node prevents the dislocations from conserving their screw orientation and that the dislocations relax to a mixed orientation in their $P_{12} = (10\bar{1})$ and $P_{34} = (101)$ glide planes, with the node producing the kinks necessary to the dislocation motion. When an external stress is applied, the kinks move to the dislocation extremities and the dislocations tend to recover their screw orientations. Then, the node produces new kinks by the same mechanism, which yields the long-range motion observed in experiments. Further analysis with anisotropic elasticity theory (Supplementary Materials) shows that the line tension exerted by the dislocations on the node is responsible for this relaxation of the dislocations from a screw to a mixed orientation and that this behaviour is generic to BCC metals. Once the dislocations have lost their screw character, they can glide without experiencing any noticeable lattice friction under a small applied stress, leading to the fast and long-distance motion observed in TEM. The four dislocations recover their screw character when they stop at an extrinsic obstacle. The node

can only glide along the $[010]$ direction defined by the intersection of the two $\{110\}$ planes, thus constraining $\vec{b}_1$ and $\vec{b}_2$ on the one hand, and $\vec{b}_3$ and $\vec{b}_4$ dislocations on the other hand, to glide respectively in P_{12} and P_{34} planes. Since the four dislocations glide cooperatively at an abnormal high velocity in planes P_{12} and P_{34} where the driving resolved shear stress is not the highest (see Extended Data Table 2 for resolved shear stresses in the different slip planes), we believe that such a highly surprising behaviour is the true origin of anomalous slip.

In situ TEM straining experiments reveal, with the help of atomistic simulations, the detailed mechanism leading to the formation and then the fast glide of such four-dislocation node (Fig. 2). The starting configuration is made of two screw dislocations $\vec{b}_1 = 1/2\,[\bar{1}1\bar{1}]$ and $\vec{b}_2 = 1/2\,[111]$ which have reacted to form a junction with Burgers vector $\vec{b}_{JR} = 1/2\,[\bar{1}1\bar{1}] + 1/2\,[111] = [010]$. Atomistic simulations (Fig. 4a and Ref. 21) and anisotropic elasticity (see Supplementary Information) show that such a reaction is energetically favourable in niobium. All dislocations, the two $\vec{b}_1$ and $\vec{b}_2$ screw dislocations and the $\vec{b}_{JR}$ junction reaction are contained in their common $P_{12} = (10\bar{1})$ slip plane. Another screw dislocation with Burgers vector $\vec{b}_3 = 1/2\,[1\bar{1}\bar{1}]$ glide in direction of the junction in the primary plane $P_{23} = (01\bar{1})$ where the resolved shear stress is maximum. Upon intersection with the junction $\vec{b}_{JR}$, both dislocations react to form a dislocation with the fourth Burger vector $\vec{b}_4 = -\vec{b}_{JR} - \vec{b}_3 = 1/2\,[\bar{1}\bar{1}1]$. Experiments do not allow imaging the reaction product of this interaction, as all dislocations on the left of the initial junction escape out of the observation zone in less than 40 ms just after the interaction, but atomistic simulations (Fig. 3a) confirm the creation of this $\vec{b}_4$ dislocation, leading to two nodes connecting four dislocations with different $1/2\,\langle 111\rangle$ Burgers vector. In the video frame just after the interaction (Fig. 2c), four new horizontal slip traces have been created on the thin foil surface and several dislocation segments have disappeared. As clearly seen on the differential image

(Fig. 2e), three of these slip traces are connected to the $\vec{b}_1$, $\vec{b}_2$, and $\vec{b}_3$ screw dislocations which have escaped to the left. The fourth slip trace on the bottom surface of the thin foil is necessary due to the glide of the $\vec{b}_4$ dislocation, as a result of the mechanism described in what follows. Once the $\vec{b}_4$ dislocation has been created by the reaction between $\vec{b}_3$ and $\vec{b}_{JR}$, this dislocation segment extends and forms a screw dislocation dipole in the P_{34} plane emerging at the bottom surface of the thin foil (Fig. 2i, j). Molecular dynamics simulations (Fig. 3b) reproduce well the bowing of this $\vec{b}_4$ dislocation under an applied stress, leading to the creation of the four-dislocation node. The whole configuration is then divided in two parts: a group of four screw dislocations connected to a node, which rapidly glide to the left, and a remaining tangle on the right (Fig. 2j, k). In the last video frame (Fig. 2d), only this tangle is present, with the $\vec{b}_4$ dislocation forming another screw dipole with a direction corresponding unambiguously to its Burgers vector and allowing its identification.

The existence of four-dislocation node in BCC metals has already been discussed by Bulatov *et al.*[3], but with dislocations belonging to three different $\{110\}$ planes intersecting along a $\langle 111 \rangle$ direction. These multi-junctions are then strong anchoring points, leading to substantial strain hardening and acting as dislocation sources. The multi-junctions observed here are different, corresponding to four dislocations belonging to two different $\{110\}$ planes intersecting along a $\langle 100 \rangle$ direction. Being highly mobile, they lead to the reverse effect and are a source of considerable softening.

These highly mobile multi-junctions offer a nice explanation to the occurrence of anomalous slip in BCC metals, starting from a large network of dislocations $\vec{b}_1$ and $\vec{b}_2$ (Extended Data Fig. 4). Such networks are created after activation of dislocations glide in their most favourable planes and result from mutual blocking of dislocations $\vec{b}_1$ and $\vec{b}_2$ which form arrays in the plane containing them. The formation of large planar arrays is helped by the

associated decrease of the elastic energy, because of a substantial twist component. Incoming dislocations $\vec{b}_3$, which glide in the primary P_{23} plane, will form many glissile multi-junctions when intersecting such networks. This will result in further glide of $\vec{b}_1$ and $\vec{b}_2$ dislocations in the P_{12} plane and in deviation of $\vec{b}_3$ dislocations from their primary to the P_{34} slip plane where they will glide with $\vec{b}_4$ dislocations. It is important to note that none of the four dislocations can cross slip during their cooperative glide motion, which results in a very planar slip in P_{12} and P_{34} planes. In this description, $\vec{b}_3$ and $\vec{b}_4$ dislocations glide in many parallel slip planes, thus producing fine slip traces, hardly visible, at the surface of the sample. On the other hand, all $\vec{b}_1$ and $\vec{b}_2$ dislocations glide in a single P_{12} plane, namely the plane of the starting network, which results in a very coarse and straight slip band characteristic of anomalous slip. This mechanism also agrees with the average shear direction intermediate between two Burgers vectors directions and with the absence of dead band usually observed in anomalous slip conditions.

$\langle 100 \rangle$ junctions resulting from the interaction of two $1/2\ \langle 111 \rangle$ screw dislocations appear an essential ingredient of anomalous slip, as they are necessary to the creation of glissile multi-junctions. According to anisotropic elasticity (Supplementary Materials and Ref. 22), such junction reactions are stabilized by a decreasing ratio of the shear moduli $A = 2C_{44}/(C_{11} - C_{12})$. This agrees with the observation[23] that activity of anomalous slip in BCC metals correlates with the anisotropic ratio A and is more prominent for small values, like in niobium ($A = 0.5$). Elasticity predicts that formation of $\langle 100 \rangle$ junctions becomes unfavourable in metals where this A ratio is larger than ~0.8. In particular, in the isotropic case of tungsten ($A = 1$), atomistic simulations confirm that the interaction of two $1/2\ \langle 111 \rangle$ screw dislocations do not spontaneously lead to the creation of a $\langle 100 \rangle$ junction (Fig. 4b). This appears in contradiction with the existence of anomalous slip in tungsten[4,5]. In situ TEM

tensile tests give the solution to this apparent paradox. Despite the energy cost of these junctions in tungsten, they can be created in dynamic conditions from two intersecting screw dislocations (Fig. 4c). TEM reveal that these dislocations glide under an applied stress only on one side of their contact point and remain immobile on the other side, thus leading to the creation and extension of a $\langle 100 \rangle$ junction. Molecular dynamics simulations (Fig. 4d) show that this dynamic creation of a $\langle 100 \rangle$ junction is a consequence of the preferential nucleation of kinks at the node[17,18] connecting the two screw dislocations leading to an increased mobility of one half of the screw dislocations. This mechanism will be less effective when the energy cost of $\langle 100 \rangle$ junction reactions becomes too high, i.e. in metals where the anisotropy ratio A is much larger than 0.8. This explains why no such $\langle 100 \rangle$ junction, and no anomalous slip, has been ever observed in iron which has the highest ratio ($A = 2.38$) among all BCC metals.

Anomalous slip observed at low temperature in BCC metals arises thus from the unusual high mobility of multi-junctions. Depending on their configuration, multi-junctions in BCC metals can be either a source of hardening as already demonstrated[3,24] or a source of softening as in the present case where anomalous slip takes place. Understanding and modelling the formation of these multi-junctions necessitates going beyond some usual simplifications in dislocation theory, with elastic anisotropy being a key ingredient and the creation in dynamic conditions of junctions which would have been found unstable with a criterion based solely on energy. Finally, our study illustrates the necessity to image in situ the motion of dislocations during deformation to fully understand dislocation interaction controlling plasticity, as these highly mobile four-dislocation nodes responsible of anomalous slip would have been absent in post-mortem observations.

References

1. Christian, J.W. Some surprising features of the plastic deformation of body-centred cubic metals and alloys. *Metall. Trans.* **14A**, 1237-1256 (1983).
2. Taylor, G. Thermally-activated deformation of BCC metals and alloys. *Prog. Mater Sci.* **36**, 29-61 (1992).
3. Bulatov, V.V., Hsiung, L.L., Tang, M., Arsenlis, A., Bartelt, M.C., Cai, W., Florando, J.N., Hiratani, M., Rhee, M., Hommes, G., Pierce, T.G. & Diaz de la Rubia, T. Dislocation multi-junctions and strain hardening. *Nature* **440**, 1174-1178 (2006).
4. Kaun, L., Luft, A., Richter, J. & Schulze, D. Slip line patterns and active slip systems of tungsten and molybdenum single crystals weakly deformed in tension at room temperature. *Phys. Stat. Sol.* **26**, 485-499 (1968).
5. Marichal, C., Srivastava, K., Weygand, D., Van Petegem, S., Grolimund, D., Gumbsch, P. & Van Swygenhoven, H. Origin of anomalous slip in tungsten. *Phys. Rev. Lett.* **113**, 025501 (2014).
6. Duesbery, M.S. & Foxall, R.A. A detailed study of the deformation of high purity niobium single crystals. *Philos. Mag.* **20**, 719-751 (1969).
7. Matsui, H. & Kimura, H. Comments on "Anomalous slip in a BCC crystal observed in computer simulation of screw dislocation motion". *Scr. Metall.* **8**, 1205-1207 (1974).
8. Vitek, V. & Taylor, G. Comment on "Anomalous slip in BCC crystals observed in computer simulation of screw dislocation motion". *Scr. Metall.* **8**, 1283-1285 (1974).
9. Saka, H., Noda, K., Imura, T., Matsui, H. & Kimura, H. HVEM in-situ observation of anomalous (101) slip in molybdenum. *Philos. Mag.* **34**, 33-48 (1976).
10. Matsui, H. & Kimura, H. Anomalous {110} slip in high-purity molybdenum single crystals and its comparison with that in V(a) metals. *Mater. Sci. Eng.* **24**, 247-256 (1976).

11. Wasserbäch, W. Anomalous slip in high-purity niobium and tantalum single crystals. *Phys. Stat. Sol. (a)* **147**, 417-446 (1995).
12. Louchet, F. & Kubin, L.P. Dislocation substructures in the anomalous slip plane of single crystal niobium strained at 50 K. *Acta Metall.* **23**, 17-21(1975).
13. Hsiung, L.L. On the mechanism of anomalous slip in BCC metals. *Mater. Sci. Eng. A* **528**, 329-337 (2010).
14. Matsui, H. & Kimura, H. A mechanism of the unexpected {110} slip observed in BCC metals deformed at low temperatures. *Scr. Metall.* **7**, 905-913 (1973).
15. Taylor, G. Comments on `a mechanism of the unexpected {110} slip observed in BCC metals deformed at low temperatures'. *Scr. Metall.* **8**, 459-461 (1974).
16. Matsui, H. & Kimura, H. Anomalous {110} slip and the role of co-planar double slip in BCC metals. *Scr. Metall.* **9**, 971-978 (1975).
17. Bulatov, V.V. & Cai, W. Nodal effects in dislocation mobility. *Phys. Rev. Lett.* **89**, 115501 (2002).
18. Yang, J.B., Zhang, Z.J. & Zhang, Z.F. Quantitative understanding of anomalous slip in Mo. *Philos. Mag.* **95**, 2026-2045 (2015).
19. Holzer, J., Chlup, Z., Kruml, T. & Gröger, R. Plastic deformation of magnetically isotropic Cr single crystals compressed at 77 K. *Int. J. Plast.* **138**, 102938 (2021).
20. Louchet, F. & Kubin, L.P. A possible explanation for the anomalous slip of BCC metals from “in situ” experiments. *Scr. Metall.* **9**, 911-916 (1975).
21. Xia, Z.Y., Zhang, Z.J., Yan, J.X., Yang, J.B. & Zhang, Z.F. Simulation of the interaction between two different 1/2<111> screw dislocations in body-centred-cubic metal niobium. *Comp. Mater. Sci.* **174**, 109503 (2020).
22. Chou, Y.T. Dislocation reactions and networks in anisotropic BCC crystals. *Mater. Sci. Eng.* **10**, 81–86 (1972).

23. Seeger, A. & Wasserbäch, W. Anomalous slip – A feature of high-purity body-centred cubic metals. *Phys. Stat. Sol. (a)* **189**, 27-50 (2002).

24. Madec, R. & Kubin, L.P. Second-order junctions and strain hardening in BCC and FCC crystals. *Scr. Mater.* **58**, 767-770 (2008).

Methods

Experiments.

Experiments have been carried out in a high-purity (5N) niobium single crystal bought at Goodfellow and in a tungsten single crystal containing less than 1 ppm of O, C, N, and Si, and less than 0.1 ppm of other elements, given by P. Gumbsch and D. Weygand and already used in previous studies[25,26].

Nb microsamples have been cut in a (501) plane with a tensile direction $T = [\bar{1}05]$ which is always vertical in the images. The direction $[010]$ corresponding to the Burgers vector of the junction JR is accordingly horizontal. As this $[010]$ direction lies in the foil plane, this makes it possible to observe the fast motion of the four-dislocation node along this direction. Otherwise the node would have rapidly disappeared at a surface. Referring to the stereographic projection in Fig. 2, dislocations with Burgers vectors $\vec{b}_1 = 1/2\ [\bar{1}1\bar{1}]$, $\vec{b}_2 = 1/2\ [111]$, $\vec{b}_3 = 1/2\ [1\bar{1}\bar{1}]$ and $\vec{b}_4 = 1/2\ [\bar{1}\bar{1}1]$ are activated in planes $P_{12} = (10\bar{1})$, $P_{34} = (101)$, and $P_{23} = (0\bar{1}1)$. Most observations are carried out with the diffraction vector $g_1 = (010)$, for which all dislocations are in contrast, but other diffracting conditions $g_2 = (011)$ and $g_3 = (0\bar{1}1)$ are also sometimes used. After complete contrast analyses, it appeared that straight screw dislocations could be easily identified via their apparent direction in projection on the screen plane.

Nb microsamples are strained in the Gatan low-temperature straining holder working at 95 K and W samples at 373 K in a high-temperature straining holder locally developed at Toulouse. Samples are observed in a JEOL 2010-HC TEM operating at 200 kV. Video sequences are recorded using a MegaView III camera at a rate of 50 images per second and analysed frame by frame.

The signs of moving dislocations, which determine their capabilities to react with each other, are unambiguously deduced from their directions of motion under the tensile applied stress.

Atomistic simulations.

Atomistic simulations have been performed using the LAMMPS code[27] with the EAM potential of Fellinger et al. for niobium[28] and the MEAM potential of Park et al. for tungsten[29]. Molecular statics relaxations are performed with the Fire algorithm[30], using a threshold criterion of 5 meV/Å on atomic forces for all Cartesian coordinates. A NVE ensemble is used for molecular dynamics simulations, with an initial thermalization stage to initialize the temperature. Constant strain rate conditions are imposed by controlling the average displacement of the upper and lower layers of the simulations cell, using the flexible boundary conditions introduced by Rodney[31].

The simulation cell used for the relaxation of the four-dislocation node (Fig. 1) is defined by the three vectors $120\ [010]$, $80\ [001]$ and $80\ [100]$ with free surfaces in all Cartesian directions. Four screw dislocation segments with Burgers vectors $\vec{b}_1 = 1/2\ [\bar{1}1\bar{1}]$, $\vec{b}_2 = 1/2\ [111]$, $\vec{b}_3 = 1/2\ [1\bar{1}\bar{1}]$ and $\vec{b}_4 = 1/2\ [\bar{1}\bar{1}1]$ are introduced so as to intersect on a node located in the simulation cell at the two thirds of the cell height in the $X \parallel [010]$ direction. The four dislocation segments come out of the simulation cell on each $[010]$ external edge.

The formation of the four-dislocation node in niobium (Fig. 3) is modelled in a simulation cell defined by $120\ [010]$, $120\ [\bar{1}01]$ and $40\ [101]$, with free surfaces in all Cartesian directions. A binary $[010]$ screw junction formed by two intersecting screw dislocation segments with Burgers vectors $\vec{b}_1 = 1/2\ [\bar{1}1\bar{1}]$ and $\vec{b}_2 = 1/2\ [111]$ is introduced piecewise in the centre of the simulation cell (Fig. 3a). The $[010]$ junction has a length of $20\ a$, with a the lattice

parameter. After relaxation of the junction, a third screw dislocation with Burgers vector $\vec{b}_3 = 1/2\ [1\bar{1}\bar{1}]$ is introduced. It intersects the $[010]$ junction in its middle. Upon relaxation, the $[010]$ junction unzips, leading to the creation of a mixed dislocation with Burgers vector $\vec{b}_4 = 1/2\ [\bar{1}\bar{1}1]$ and of length $20\ a$ (Fig. 3a). The bow-out of this $\vec{b}_4$ dislocation (Fig. 3b) is simulated with molecular dynamics simulations in the same simulation cell, but for an initial length $80\ a$ of this $\vec{b}_4$ dislocation. The temperature is $T = 200$ K and the strain rate $\dot{\varepsilon}_{xz} = 5.6 \times 10^7$ s^{-1}.

The simulation cell used to study the formation of the $[010]$ junction in Nb and W (Fig. 4) is defined by the vectors $140\ [010]$, $100\ [\bar{1}01]$ and $30\ [101]$, with periodic boundary conditions along the first direction and free surfaces for the two other directions. Two screw dislocations with Burgers vectors $\vec{b}_1 = 1/2\ [\bar{1}1\bar{1}]$ and $\vec{b}_2 = 1/2\ [111]$, which intersect in the centre of the simulation cell, are introduced. Relaxation by molecular statics leads to the spontaneous creation of a $[010]$ junction in Nb (Fig. 4a), but not in W (Fig. 4b). The molecular dynamics simulations showing the dynamical creation of a $[010]$ junction in W are performed at $T = 200$ K and at a strain rate $\dot{\varepsilon}_{xz} = 4.7 \times 10^7$ s^{-1}.

References for Methods section

25. Brunner, D. Comparison of flow-stress measurements on high-purity tungsten single crystals with the kink-pair theory. *Mater. Trans. JIM* **41**, 152-160 (2000).
26. Caillard, D. Geometry and kinetics of glide of screw dislocations in tungsten between 95K and 573K. *Acta Mater.* **161**, 21-34 (2018).
27. Plimpton, S. Fast parallel algorithms for short-range molecular dynamics. *J. Comput. Phys.* **117**, 1-19 (1995).

28. Fellinger, M.R., Park, H. & Wilkins, J.W. Force-matched embedded-atom method potential for niobium. *Phys. Rev. B* **81**, 144119 (2010).
29. Park, H., Fellinger, M.R., Lenosky, T.J., Tipton, W.W., Trinkle, D.R., Rudin, S.P., Woodward, C., Wilkins, J.W. & Hennig, R.G. Ab initio based empirical potential used to study the mechanical properties of molybdenum. *Phys. Rev. B* **85**, 214121, (2012).
30. Bitzek, E., Koskinen, P., Gähler, F., Moseler, M. & Gumbsch, P. Structural relaxation made simple. *Phys. Rev. Lett.* **97**, 170201 (2006).
31. Rodney, D. Activation enthalpy for kink-pair nucleation on dislocations: Comparison between static and dynamic atomic-scale simulations. *Phys. Rev. B* **76**, 144108 (2007).

Acknowledgements

Atomic simulations in this work were performed using HPC resources from GENCI-CINES and -TGCC (Grants 2021-096847). B.B. and E.C. acknowledge funding by the French Tripartite Institute (CEA-EDF-Framatome) through the ICOMB project.

Author contributions

D.C. designed the study and performed the in situ TEM straining experiments. B.B. and E.C. performed the atomistic simulations and developed the elastic model. All the authors discussed the results, prepared the manuscript and reviewed the paper.

Figures

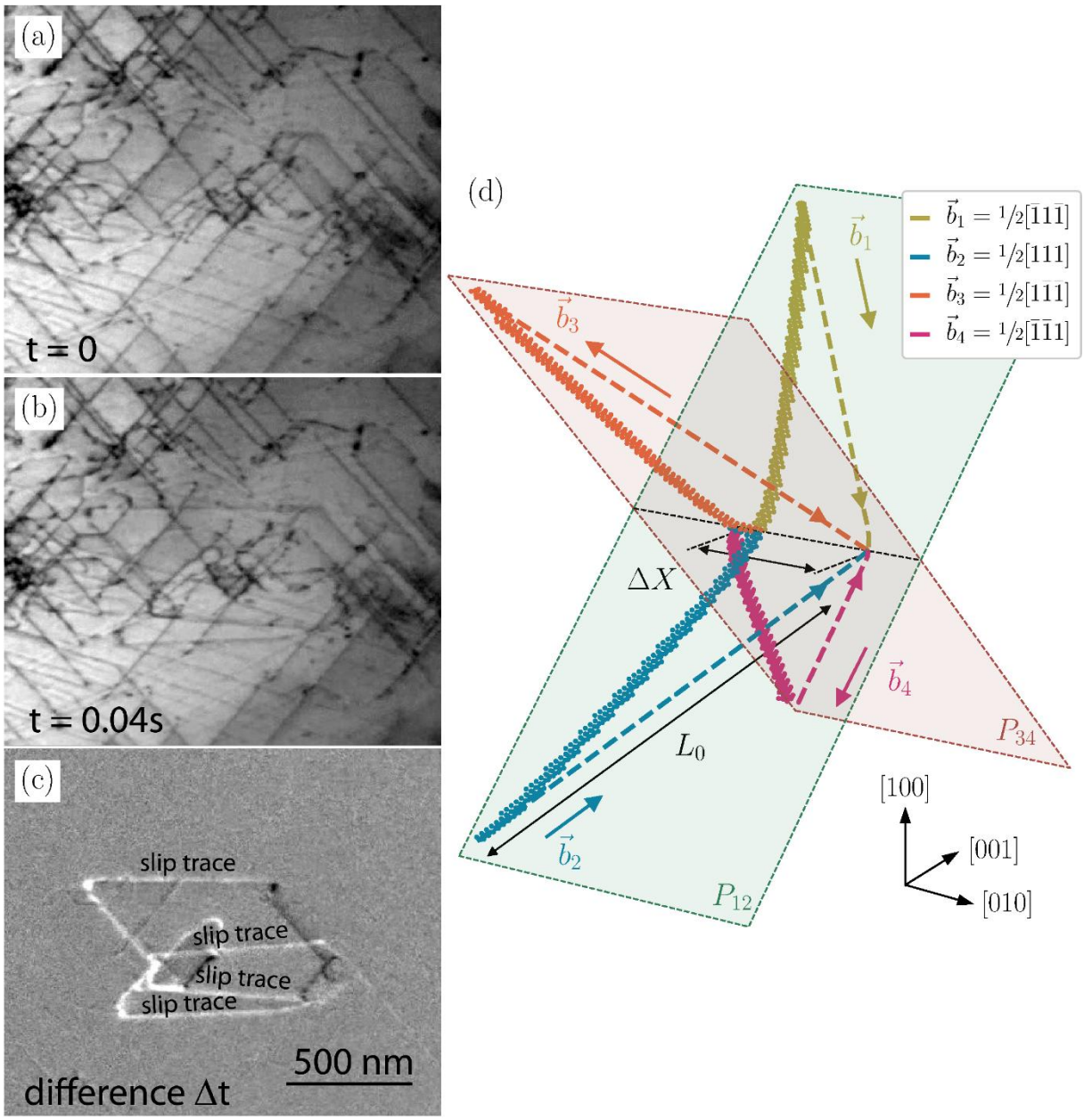

Figure 1: Rapid glide of a node connecting four screw dislocations in niobium.

The same dislocation network is imaged in a and b at two different times. The image c is obtained by taking the difference between these two frames and enlightens the dislocations motion in the time interval with initial and final positions appearing respectively in black and white. Four screw dislocations have glided cooperatively on a large distance in less than 40 ms and have created two sets of slip traces on the two foil surfaces corresponding to planes

$P_{12} = (10\bar{1})$ and $P_{34} = (101)$, clearly visible as horizontal lines with a white contrast in the image difference c. (d) Atomistic simulations of the corresponding node connecting four screw dislocations of length L_0. Upon relaxation, the node glides along the $[010]$ direction over a distance ΔX and the dislocations, which are anchored at their other extremity by the surface, lose their initial screw orientations indicated by dashed lines. Anisotropic elasticity theory shows that this relaxation distance ΔX is proportional to the length L_0 of the initial screw segments and is controlled by the anisotropy of the elastic constants. Coloured spheres correspond to atoms belonging to the relaxed dislocation cores.

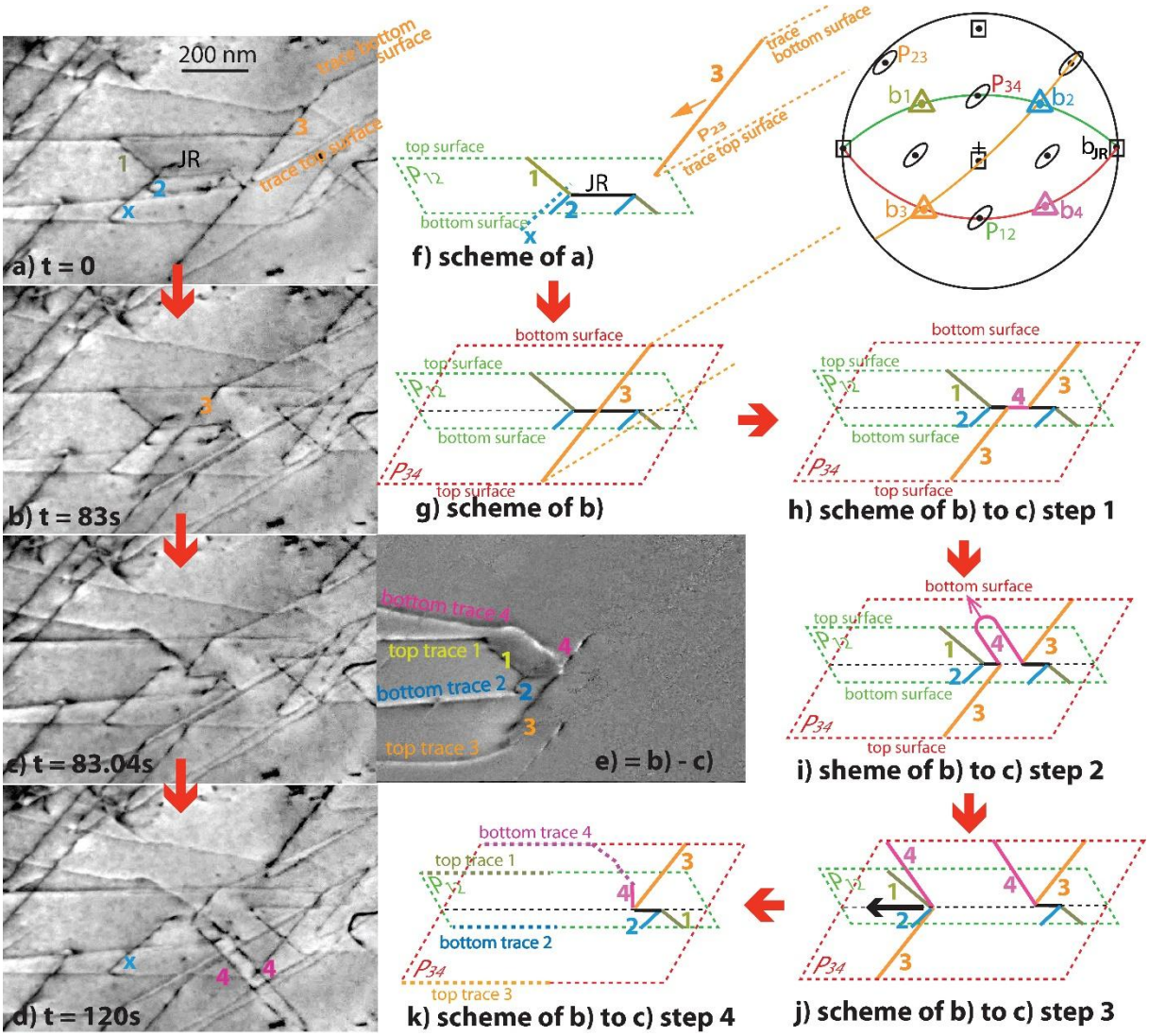

Figure 2: Formation and rapid glide of a four-dislocation node in niobium.

The observed time sequence **(a-d)** and its schematic description **(f-k)** show the detailed mechanism leading to the formation of a node connecting four screw dislocations and its rapid glide out of the observation zone. The starting configuration in **(a)** is made of two screw dislocations $\vec{b}_1 = 1/2\,[\bar{1}1\bar{1}]$ and $\vec{b}_2 = 1/2[111]$ reacting to form a junction JR with Burgers vector $\vec{b}_{JR} = [010]$. The three dislocations are contained in their common slip plane $P_{12} = (10\bar{1})$. Another screw dislocation $\vec{b}_3 = 1/2\,[1\bar{1}\bar{1}]$ glides to the bottom left in its slip plane $P_{23} = (0\bar{1}1)$ and intersects in **(b)** the junction reaction JR. In the next frame **(c)**, separated from the previous one by only 40 ms, the investigated process has already occurred, with the creation of four slip traces corresponding to glide planes $P_{12} = (10\bar{1})$ and $P_{34} = (101)$ and the disappearance of several dislocation segments. The image difference **(e)** allows connecting these slip traces to the glide of the three previous screw dislocations and an

additional dislocation $\vec{b}_4 = 1/2[\bar{1}\bar{1}1]$, which results from the reaction between $\vec{b}_3$ and the junction reaction JR, as sketched in **(h)**. This fourth dislocation extends and form in the plane P_{34} a screw dipole **(i)** which emerges at the bottom surface **(j)**. The whole configuration is then divided in two parts, a group of four screw dislocations connected to a node which rapidly glides to the left out of the observation zone and a remaining tangle on the right **(k),** where the screw segment 4 has shortened its length by cross-slip. The last image **(d)** shows the subsequent evolution of the short segment 4 forming another screw dipole which is used to check that the dislocation 4 has the expected Burgers vector $\vec{b}_4$.

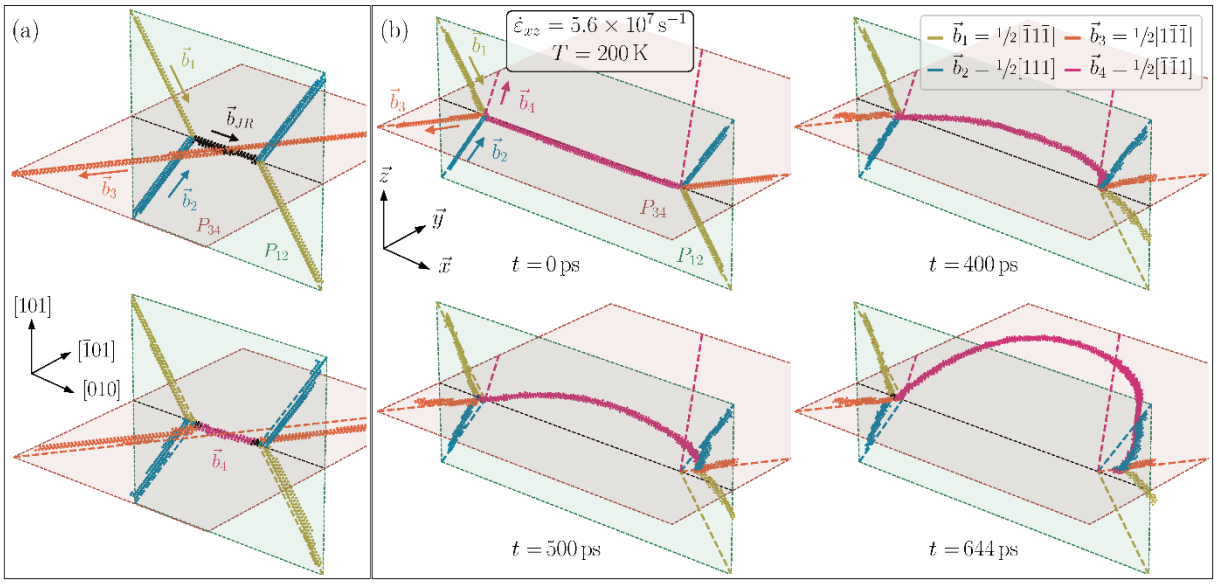

Figure 3: Atomistic simulations of the formation of a four-dislocation node in niobium.

(a) A $\vec{b}_3 = 1/2\,[\bar{1}1\bar{1}]$ screw dislocation reacts with a $\vec{b}_{JR} = [010]$ junction formed by two screw dislocations, $\vec{b}_1 = 1/2\,[\bar{1}1\bar{1}]$ and $\vec{b}_2 = 1/2[111]$. Upon relaxation by molecular statics, a mixed $\vec{b}_4 = 1/2[\bar{1}\bar{1}1]$ dislocation is formed, leading to two nodes connecting four different $1/2\langle 111\rangle$ dislocations. (b) Upon straining in molecular dynamic simulations, the mixed $\vec{b}_4$ dislocation bows out and tends to its screw orientation (dashed lines) close to the nodes which start to glide.

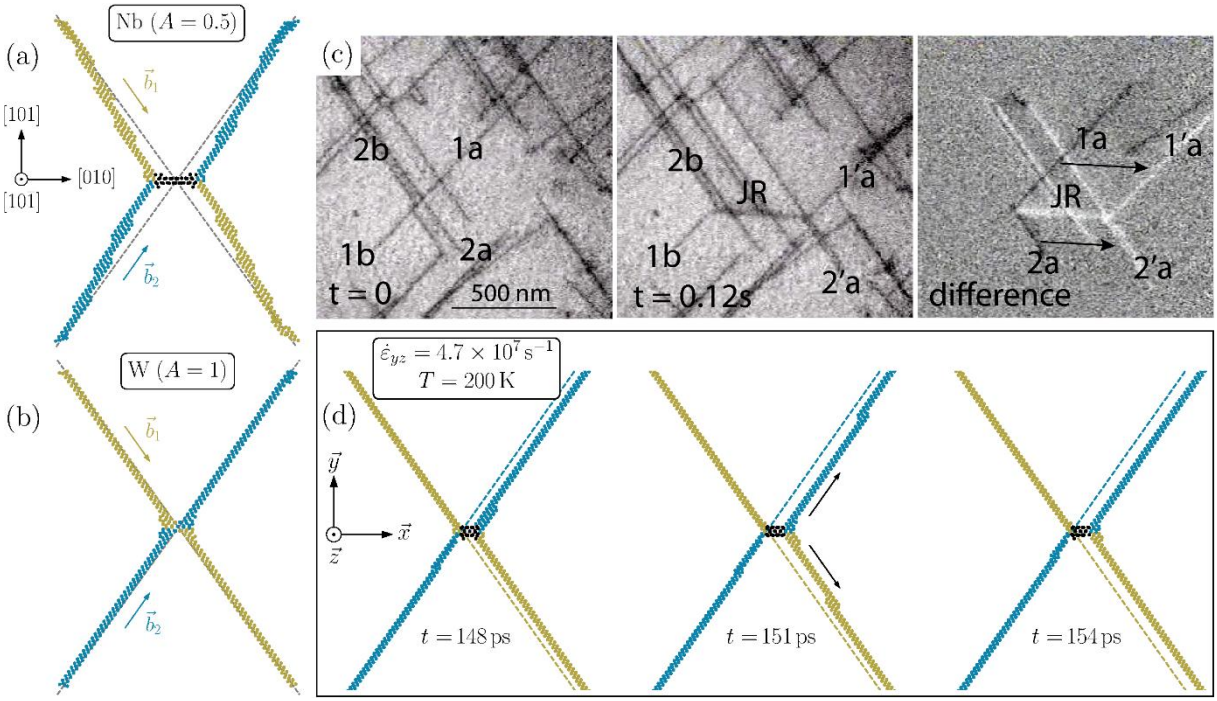

Figure 4: Formation of a [010] junction by intersection of two 1/2⟨111⟩ screw dislocations.

Atomistic simulations show (a) the spontaneous formation of the junction in niobium, whereas (b) no junction appears by relaxation in tungsten. (c) Formation of [010] junction can nevertheless be observed in tungsten by TEM with in situ straining experiments at 373 K. Two intersecting screw dislocations with different 1/2⟨111⟩ Burgers vector are observed at two different times. The difference image between the two frames shows that the right parts of the screw dislocations noted 1a and 2a have glided to the right while their left parts 1b and 2b remain fixed leading to the creation of the junction JR. (d) Molecular dynamics simulations show that this dynamical creation of a [010] junction in tungsten operates through the nucleation of kinks at the node on the right dislocation segments.

Extended Data

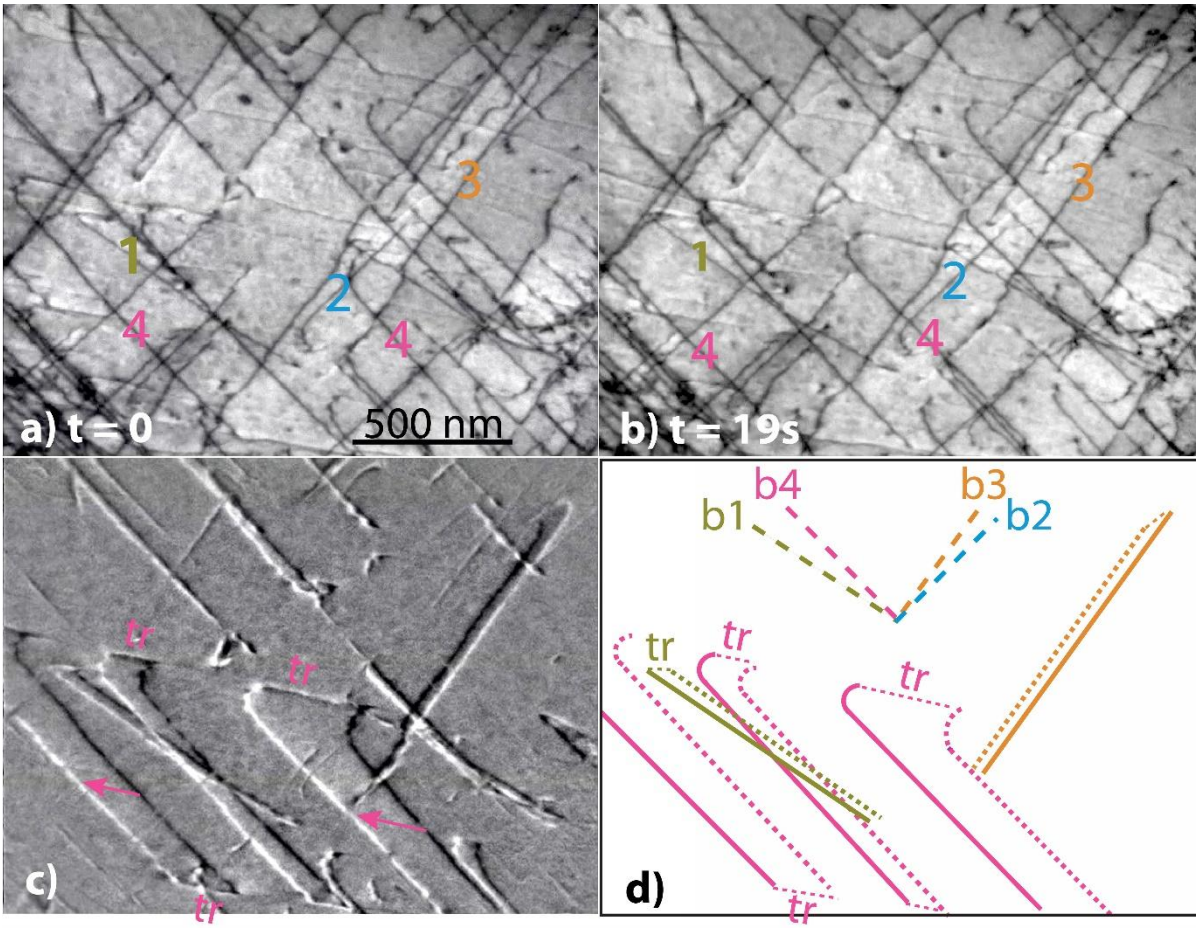

Extended Data Figure 1: Glide of isolated screw dislocations in niobium.

The frames a) and b) follow the motion of the same dislocations at two different times. The image c) is obtained by taking the difference between these two frames and enlightens the dislocations motion in the time interval with initial and final positions appearing respectively in black and white. This dislocation motion is sketched in frame d) with initial and final positions of gliding dislocation drawn respectively with solid and dashed lined. The slip traces left on the thin foil surface by the gliding dislocations, noted 'tr', correspond to non-crystallographic slip planes. The dislocations straighten along their screw orientation when gliding with a slow and steady motion at an average velocity of the order of 5 nm/s. Four

dislocation families with different Burgers vectors $\vec{b}_1$, $\vec{b}_2$, $\vec{b}_3$, and $\vec{b}_4$ are identified and can be distinguished in the images thanks to their different directions and lengths in projection.

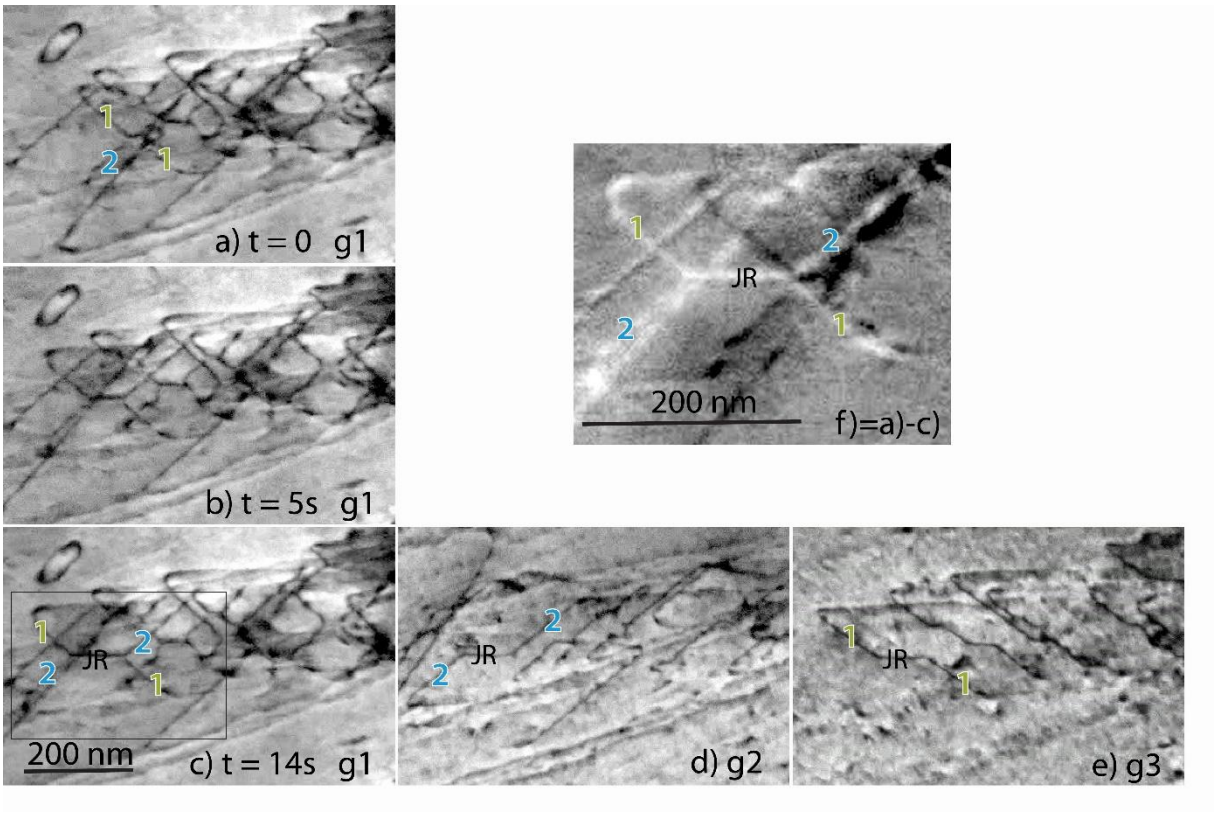

Extended Data Figure 2: Glide of a dislocation network in niobium.

The same dislocation network is imaged in a) to c) at 3 different times, using the diffraction vector $g_1 = (010)$. Two other diffraction vectors, $g_2 = (011)$ and $g_3 = (0\bar{1}1)$, are used in d) and e) to determine Burgers vectors by extinction just after time t = 14 s as in c). The network is made of two interacting screw dislocation families with Burgers vectors $\vec{b}_1 = 1/2\,[\bar{1}1\bar{1}]$ and $\vec{b}_2 = 1/2[111]$, forming horizontal junctions with Burgers vector $\vec{b}_{JR} = [010]$ through the reaction $1/2\,[\bar{1}1\bar{1}] + 1/2[111] = [010]$. This network glides in the average plane $P_{12} = (10\bar{1})$ containing the three dislocation families, leading to the horizontal slip traces visible in all images, especially in e) with diffraction vector g_3 where dislocations 2 are out of contrast. The slip traces are clearly distinct for different emerging dislocations 1 and 2, which shows that the network is not entirely contained in a single P_{12} plane. The image difference f) between a) and c) highlights the motion of the fastest node of the network, leading to a velocity of about 15 nm/s.

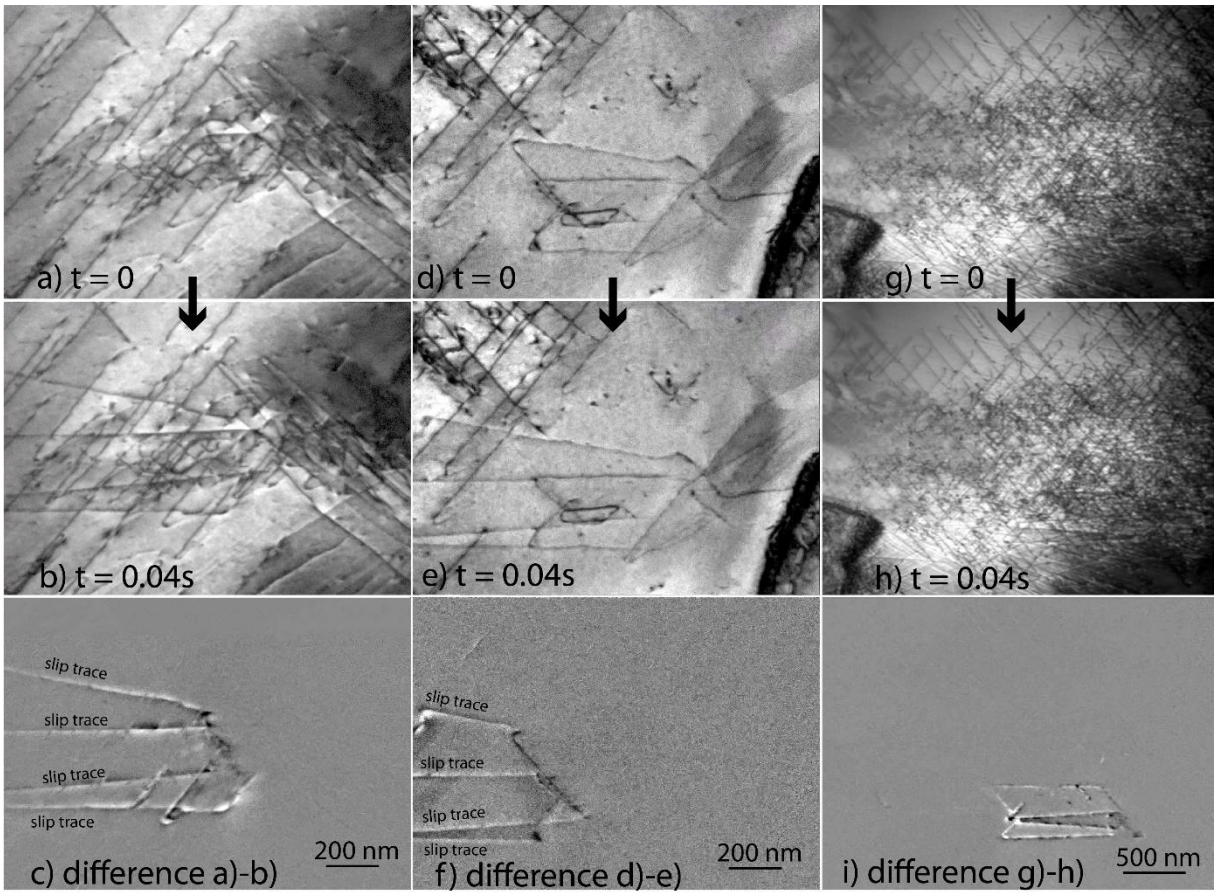

Extended Data Figure 3: Rapid glide of a node connecting four screw dislocations in niobium.

Three different events are shown, all corresponding to the same mechanism as in Figures 1 and 2 of the main text where four screw dislocations connected to a node glide in two different planes over a large distance in less than 40 ms. The event a)-b) has been obtained in the same area as in Fig. 2 after further deformation. The second set d)-e) has been obtained in the same sample in a neighbouring area and precedes the event described in Fig. 2 in the main text. The last event d)-h) comes from the same sample as the one described in Fig. 1 in the main text after a rather large amount of deformation. The two sets of traces are remarkably similar for each sample, namely c and f on one hand, i and Fig. 1c of the main text on the other hand.

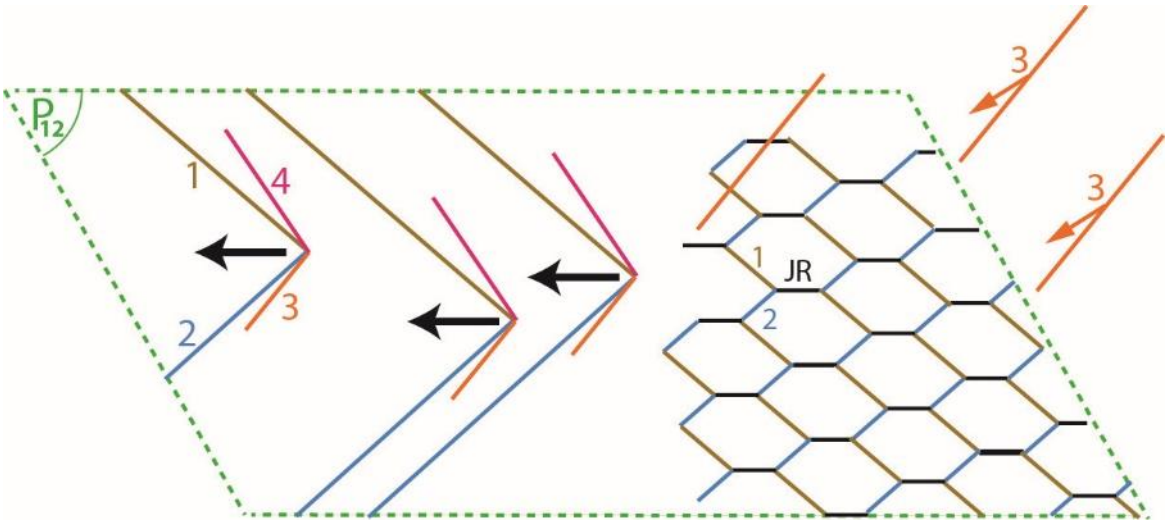

Extended Data Figure 4: Mechanism leading to anomalous slip.

A network formed by $\vec{b}_1$ and $\vec{b}_2$ screw dislocations in P_{12} plane is intersected by dislocations $\vec{b}_3$ which glide in the principal slip system. The interaction results in the creation of highly mobile junctions, leading to long-distance glide of $\vec{b}_1$ and $\vec{b}_2$ dislocations in a single P_{12} plane and of $\vec{b}_3$ and $\vec{b}_4$ dislocation in many parallel slip P_{34} planes.

Metal	*Deformation mode*	*Athermal temperature of the Peierls mechanism*	*Temperature range of anomalous slip, most relevant in red (temperature range investigated between brackets)*	*Dislocation activity*	*Orientation of the tension/compression axis in the elementary stereographic triangle*	*Ref.*
V	*compression*	*Ta # 400K [32]*	*77-173K (77-295K)*	*No dead band*	*centre and close 001*	*[33]*
	tension		*77K (77-298K)*			*[34]*
	tension		*77K (77K)*	*No dead band*	*between centre and 001*	*[35]*
Nb	*?*	*Ta=300K [42,43]*	*?*	*?*	*?*	*[6]*
	tension-compression		*77K (77K)*			*[36]*
	tension		*4.2K-77K (4.2-77K)*		*between centre and 001*	*[37]*
	tension		*50K*	*Two b's*	*close 001*	*[12]*
	tension		*77K (77K)*	*No dead band*	*centre and close 001*	*[38]*
	tension-compression		*below 200K (77-473K)*	*No dead band two b's*	*centre and between centre and 001*	*[39]*
Mo	*tension*	*Ta=450K [44,45,46]*	*300K (300K)*	*Two b's*	*centre*	*[4]*
	compression		*300K (300K)*	*Two b's*	*centre*	*[13]*
	tension		*77 K (77K)*	*Two b's*		*[10]*
Ta	*tension-compression*	*Ta=400K [40,47,48]*	*77K (77-500K)*	*No dead band*	*centre and between centre and 001*	*[39]*
	tension-compression		*4.2K-77K (4.2-450K)*		*close 001*	*[40]*
	tension-compression		*77K (77-293K)*		*centre and close 001 in tension*	*[41]*
W	*tension*	*Ta=600K [49,50]*	*300K (300K)*		*centre*	*[4]*
	compression		*300K (300K)*		*centre [-150]*	*[5]*
Cr	*compression*	*Ta=400K [51]*	*77K (77K)*		*centre*	*[19]*

Extended Data Table 1: Experimental observation of anomalous slip in different pure BCC metals.

V, Nb and Mo exhibit similar properties, namely (i) anomalous slip slightly below the athermal temperature of the Peierls mechanism, i.e. in a large part of the temperature domain of the Peierls mechanism, and (ii) evidences of two dislocation families in the anomalous plane either by TEM (noted "two b's") or via slip line observations showing no dead band (noted "no dead band"). Anomalous slip is similar but appears a little bit more difficult in Ta where lower temperatures are required, namely temperatures substantially lower than the athermal temperature of the Peierls mechanism. This latter difference appears clearly in the direct comparison of Nb and Ta by Wasserbäch[39]. For W, anomalous slip is reported in the work of Kaun et al.[4], although the term was not yet established, and more recently in the work of Marichal et al.[5]. Anomalous slip has been observed only very recently in Cr by Holzer et al.[19]. Remarkably, Fe exhibits no anomalous slip at all.

Slip direction	Slip plane	Schmid factor
$\vec{b}_1 = 1/2[\bar{1}1\bar{1}]$	$P_{13} = (110)$	0.063
$\vec{b}_3 = 1/2[1\bar{1}\bar{1}]$	$P_{13} = (110)$	0.094
$\vec{b}_2 = 1/2[111]$	$P_{24} = (101)$	0.063
$\vec{b}_4 = 1/2[\bar{1}\bar{1}1]$	$P_{24} = (101)$	0.094
$\vec{b}_3 = 1/2[1\bar{1}\bar{1}]$	$P_{34} = (101)$	0.377*
$\vec{b}_4 = 1/2[\bar{1}\bar{1}1]$	$P_{34} = (101)$	0.377*
$\vec{b}_1 = 1/2[\bar{1}1\bar{1}]$	$P_{12} = (10\bar{1})$	0.377*
$\vec{b}_2 = 1/2[111]$	$P_{12} = (10\bar{1})$	0.377*
$\vec{b}_1 = 1/2[\bar{1}1\bar{1}]$	$P_{14} = (011)$	0.314
$\boldsymbol{\vec{b}_4 = 1/2[\bar{1}\bar{1}1]}$	$\boldsymbol{P_{14} = (011)}$	**0.471**
$\vec{b}_2 = 1/2[111]$	$P_{23} = (01\bar{1})$	0.314
$\boldsymbol{\vec{b}_3 = 1/2[1\bar{1}\bar{1}]}$	$\boldsymbol{P_{23} = (01\bar{1})}$	**0.471**

Extended Data Table 2: Schmid factors of the different slip systems for a $[\bar{1}05]$ tensile axis.

The resolved shear stress for a slip system with a Schmid factor f is $\tau = f\,\sigma$, with σ the tensile stress applied along $[\bar{1}05]$ axis. The slip systems, which are easier to activate, are the ones with the highest Schmid factors. The maximum Schmid factors are obtained for dislocations $\vec{b}_3$ and $\vec{b}_4$ gliding respectively in P_{23} and P_{14}, thus defining the primary slip systems (in bold). In situ TEM tensile experiments (Figs. 1 and 2) show that the same $\vec{b}_3$ and $\vec{b}_4$ dislocations glide in P_{34}, despite the lowest Schmid factor (indicated by a *) and that $\vec{b}_1$ and $\vec{b}_2$ dislocations glide in P_{12} (also indicated by a *).

References for Extended data

32. Harrod, D.L. & Gold, R.E. Mechanical properties of vanadium and vanadium-based alloys. *Int. Met. Rev.* **25**, 1 (1980).
33. Creten, R., Bressers, J. & De Meester, P. Anomalous slip in high-purity vanadium crystals deformed in compression. *Mater. Sci. Eng.* **19**, 51-53 (1977).
34. Bressers, J. & De Meester, P. Slip plane choice in vanadium at deformation temperatures $T \leq 0.15T_m$. *J. Less-Common Met.* **84**, 11-23 (1982).
35. Taylor, G., Bajaj, R. & Carlson, O.N. Anomalous slip in high-purity vanadium crystals. *Philos. Mag.* **28**, 1035-1042 (1973).
36. Bolton, C.J. & Taylor, G. Anomalous slip in high-purity niobium single crystals deformed at 77K in tension. *Philos. Mag.* **26**, 1359-1376 (1972).
37. Aono, Y., Kuramoto, E. & Kitajima, K. Orientation dependence of slip in niobium single crystals at 4.2K and 77K. *Scripta Metall.* **18**, 201-205 (1984).
38. Wasserbäch, W. & Novak, V. Optical investigation of anomalous slip-line patterns in high-purity niobium and tantalum single crystals after tensile deformation at 77K. *Mater. Sci. Eng.* **73**, 197-202 (1985).
39. Wasserbäch, W. Anomalous slip in high-purity niobium and tantalum single crystals. *Phys. Stat. Sol. (a)* **147**, 417-446 (1995).
40. Takeuchi, S. Kuramoto, E. & Suzuki, T. Orientation dependence of slip in tantalum single crystals. *Acta Metall.* **20**, 909-915 (1972).
41. Nawaz, M.H.A. & Mordike, B.L. Slip geometry of tantalum and tantalum alloys. *Phys. Stat. Sol. (a)* **32**, 449-458 (1975).
42. Takeuchi, S., Hashimoto, T. & Maeda, K. Plastic deformation of BCC metal single crystals at very low temperatures. *Trans. Japan Inst. Met.* **23**, 60-69 (1982).

43. Ackermann, F., Mughrabi, H. & Seeger, A. Temperature and strain-rate dependence of the flow stress of ultrapure niobium single crystals in cyclic deformation. *Acta Metall.* **31**, 1353-1366 (1983).

44. Suzuki, T., Koizumi, H. & Kirchner, H.O.K. Plastic flow stress of BCC. transition metals and the Peierls potential. *Acta Metall.* **43**, 2177-2187 (1995).

45. Liu, G.C., Lau, S.S. & Dorn, J.E. The plastic deformation behavior of Mo single crystals under compression. *Phys. Stat. Sol. (a)* **11**, 645-651 (1972).

46. Guiu F. & Pratt, P.L. The effect of orientation on the yielding and flow of molybdenum single crystals. *Phys. Stat. Sol. (b)* **15**, 539-552 (1966).

47. Arsenault, R.J. An investigation of the mechanism of thermally activated deformation in tantalum and tantalum-base alloys. *Acta Metall.* **14**, 831-838 (1966).

48. Werner, M. Temperature and strain-rate dependence of the flow stress of ultrapure tantalum single crystals. *Phys. Stat. Sol. (a)* **104**, 63-78 (1987).

49. Brunner, D. Temperature dependence of the plastic flow of high-purity tungsten single crystals. *Int. J. Mate. Res.* **101**, 1003-1013 (2010).

50. Schnitzel, R.H. Deformation of tungsten single crystals from 77°C to 800°C. *J. Less Common Met.* **8**, 81–89 (1965).

51. Marcinkowski, M.J. & Lipsitt, H.A. The plastic deformation of chromium at low temperatures. *Acta Metall.* **10**, 95-111 (1962).